ELSEVIER

Robotics and Autonomous Systems 21 (1997) 23–35

Robotics and Autonomous Systems

The dynamic approach to autonomous robotics demonstrated on a low-level vehicle platform

Estela Bicho [a,b,1], Gregor Schöner [b,*]

[a] *Departamento de Electrónica Industrial, Universidade do Minho, Braga-Guimarães, Portugal*
[b] *Centre de Recherche en Neurosciences Cognitives, CNRS 13402 Marseille Cédex 20, France*

Abstract

The dynamic approach proposes a set of concepts with the help of which autonomous systems can be specified and designed. While the approach builds systems from elementary behaviors driven by behavior-specific sensory information, it also represents behaviors internally in terms of the state of dynamical systems, thus positioning itself somewhere between classical and behavior-based approaches. This paper demonstrates that the dynamic approach lends itself naturally to implementation on computationally weak platforms working with very low-level sensory information. Obstacle avoidance and target acquisition are implemented on a micro-controller based vehicle equipped with only five infra-red detectors and two photoresistors. We show how theoretical design, software simulation, and hardware implementation are enchained effortlessly. The resulting behavior is particularly smooth and requires no parameter optimization. As a technical novelty we demonstrate the integration of dynamics at two different levels of temporal derivative.

Keywords: Dynamic approach to autonomous robotics; Obstacle avoidance; Target acquistion; Low-level platforms

1. Introduction

Over the last few years autonomous robotics has experienced conceptual shifts that resulted from the tension between the classical and the behavioral approaches. The classical approach provides clear interfaces between different components by structuring robot systems along the flow of information from sensors to effectors. Information from sensory sources is extracted and represented explicitly to enable planning. Plans are acted out using well-established principles of control. By contrast, behavior-based robots use sensory information at lower levels of parameter extraction, which, typically, are not explicitly represented. Action is not explicitly planned, but emerges from the activation of prestructured elementary behaviors. (Critical discussion see, e.g., [2,3]). The dynamic approach to autonomous robotics [9–11] was developed, in part, in response to this conceptual shift. The main ideas are (see [10] for recent review): (1) Behaviors are generated by ascribing values in time to *behavioral variables*. These variables are chosen such that tasks can be expressed as values (or sets of values) of these variables. An additional constraint is the capability to enact these variables both in terms of being able to design control systems that impose the values of the variables on an effector system and in terms of being able to obtain the information that is required to define the variables from sensory surfaces.

* Corresponding author. Tel.: +33 91 164308; fax: +33 91 774969; e-mail: gregor@lnf.cnrs-mrs.fr.

[1] E-mail: estela@dei.uminho.pt.

0921-8890/97/$17.00 © 1997 Elsevier Science B.V. All rights reserved
PII S0921-8890(97)00004-3

(2) The time courses of the behavioral variables are obtained as attractor solutions of dynamical systems, the *behavioral dynamics*, formulated to express the task constraints through attractive or repulsive forces. By design, that is, through choice of variables and adjustment of time scales, the system is at all times in or near an attractor. (3) Sensory information or information from other behavioral modules (dynamical systems of other behavioral variables) determine the location, strength, and range of attractive or repulsive contributions to the behavioral dynamics. The interplay between multiple contributions to the behavioral dynamics determines how sources of sensory information may cooperate or compete which may lead to categorical change of behavior or to smooth tuning of behavior. Because behavior is always generated from attractors of nonlinear dynamical systems, powerful theoretical tools from the mathematical theory of dynamical systems, such as local bifurcation analysis, can be used to design autonomous robot architectures and quantitatively evaluate their compliance with specifications.

The dynamic approach shares with the behavioral approach the use of task-specific sensory information at low levels of invariance as well as the idea of designing systems in terms of elementary behaviors. More in line with the classical approach is the concept of representing the desired or planned behavior internally through the behavioral variables. This concept and the mathematics of dynamical systems emphasize design, specification and theoretical penetration of the architecture rather than invoking some form of emergence of behaviors as sometimes argued for behavior-based systems. The approach is open toward explicit representation of information not currently available at the sensory surfaces [4,12].

Previous implementations of autonomous robot architectures based on the dynamic approach [6,10] involved relatively large scale platforms with several on-board and off-board computer systems. Sensory information was visual, required extensive computation and potentially provided high precision information (although this potential was not always realized). In this paper we address the obvious question, if the approach is essentially limited to this type of system, more in line with the classical approach, or if, reversely, it can be made to function in computationally modest systems based on very low-level sensory information, more in line with the behavior-based approach. To demonstrate that the approach can be usefully employed on low-level systems we designed, simulated, and implemented obstacle avoidance and target acquisition on one of the simplest platforms on the market, a "rug-warrior" type microcontroller-based vehicle [5], whose sensors consist of five infra-red detectors and two light-dependent resistors. Obstacle avoidance was based on using the infra-red detectors as (uncalibrated) distance sensors. Target acquisition consisted of photo taxis (movement toward light sources) and was based on the two light-dependent resistors. The smooth and reliable performance obtained, but also the ease of the transition from theory and simulation to implementation in hardware convinced us, that the dynamic approach offers specific advantages also at this low end of the autonomous systems field.

A second, more technical aspect of this project was to establish how constraints arising at different orders of temporal derivative can be integrated. Specifically, inputs from an obstacle avoidance module arising at the level of heading direction and inputs from a target acquisition module arising at the level of the rate of change of heading direction are integrated in a single dynamical system.

Fig. 1 shows the platform we worked on, based on the MC68HCA11A0 micro-controller with 32 Kbyte of RAM, programmable in interactive C (compiler provided through the MIT Media Lab, written by Randy Sargent with the assistance of Fred Martin). The vehicle is propelled by two wheels, each driven by a simple uncontrolled motor, and stabilized by a

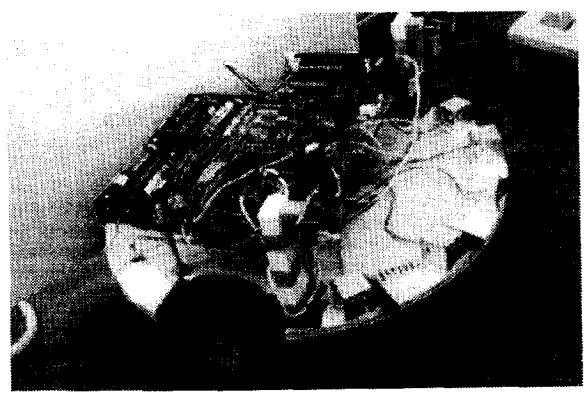

Fig. 1. The hardware platform.

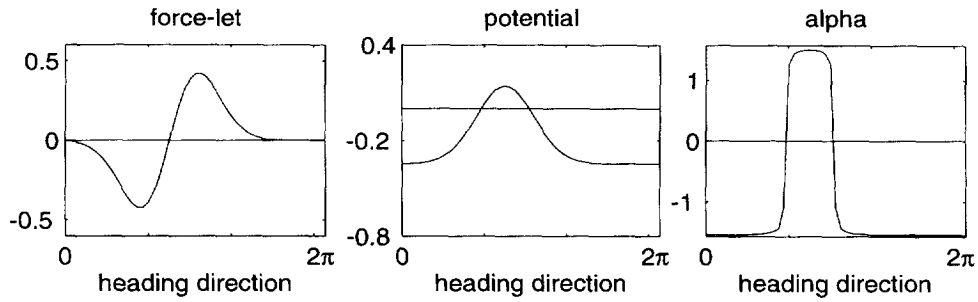

Fig. 2. Left: "Force-let" for repulsion from a heading direction in which obstructions are detected with limited range and strength: The positive slope (strength) at the zero crossing (direction to-be-avoided) indicates a repellor. Middle: Its integral provides a potential which is maximal near heading directions to-be-avoided. Right: The thresholded potential, α, serves as an indicator function of those intervals of heading direction from which obstacle forces repel.

passive caster wheel. Five active beam infra-red detectors (IRs) served for obstacle detection and two photoresistors (LDRs) provided information for the photo-taxis like target acquisition. Neither motors nor sensors were calibrated other than through rough order-of-magnitude estimation.

2. Obstacle avoidance dynamics

For obstacle avoidance a solution within the dynamic approach has been elaborated previously [9,10]. Using heading direction of the vehicle, ϕ, in an arbitrary, but fixed world reference frame, repulsive "force-lets", are defined around each direction in which obstructions are sensed. These are characterized by (a) the direction, ψ_i, to be avoided, (b) the strength, λ_i, of repulsion, and (c) the range, σ_i, over which repulsion acts. This approach can be straightforwardly transferred to the present platform by erecting repulsive force-lets (Fig. 2 left)

$$f_{\mathrm{obs},i}(\phi) = \lambda_i(\phi - \psi_i)\exp\left[-\frac{(\phi-\psi_i)^2}{2\sigma_i^2}\right] \tag{1}$$

around each direction in space, $\psi_i = \theta_i + \phi$, into which an IR sensor, mounted at angle θ_i from the frontal direction, is pointing. The strength of repulsion, λ_i, is a decreasing function of sensed distance, d_i, to the obstruction, as estimated from the IR output with crude calibration. The functional form

$$\lambda_i = \beta_1 \exp[-d_i/\beta_2] \tag{2}$$

depends on two parameters controlling the overall strength (β_1) and spatial rate of decay (β_2). The range

$$\sigma_i = \arctan\left[\tan\left(\frac{\Delta\theta}{2}\right) + \frac{R_{\mathrm{robot}}}{R_{\mathrm{robot}} + d_i}\right] \tag{3}$$

is adjusted taking both sensor sector, $\Delta\theta$, and the minimal passing distance of the vehicle (at size R_{robot} of the platform) into account. Formally, this form of the obstacle avoidance dynamics reads:

$$\dot{\phi} = F_{\mathrm{obs}} = \sum_i f_{\mathrm{obs},i}. \tag{4}$$

Note that the right-hand side really only depends on the distance measures, d_i, obtained from the sensors, not actually on ϕ (to see this, replace $\phi - \psi_i$ by θ_i, which is fixed).

We found both in simulation and in implementation that this approach to obstacle avoidance works very well, leading to particularly smooth maneuvers which are suggestive of a capacity to "plan ahead", although the dynamics are based entirely on instantaneous and local information, of course. This is illustrated in Fig. 5(a) which shows a trajectory of the simulated robot dynamics of Eq. (4). Because sensory information is used at a particularly low level, the sensor model of the simulation consists simply of a monotonic function mapping distance onto a sensor reading.

It turns out to be more difficult, however, to express photo-taxis at this level: The difference of light intensity sensed on either side of the vehicle does not specify a direction toward which to move in the absence of a world model (of the light source and the

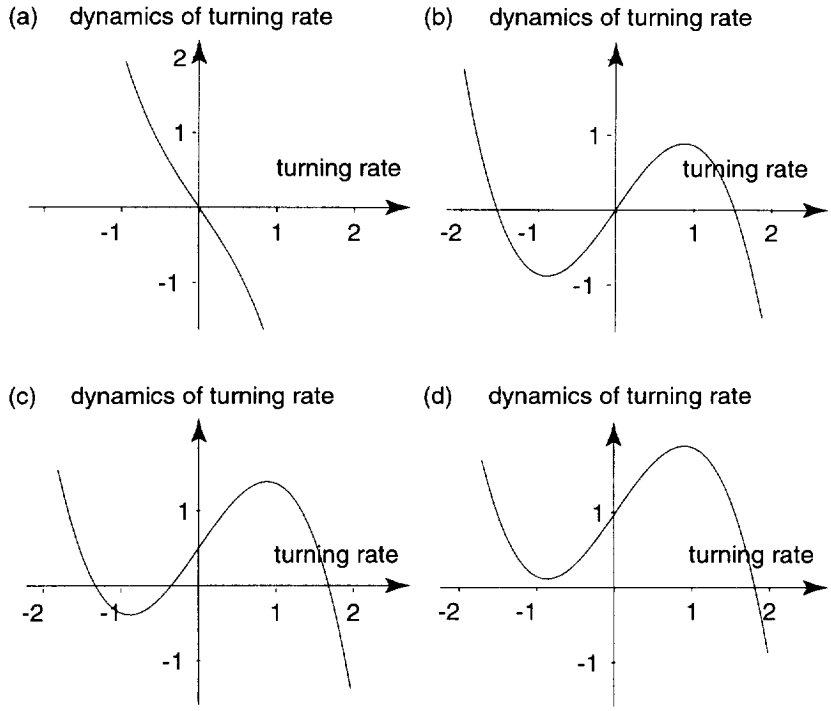

Fig. 3. The dynamics of turning rate for obstacle avoidance are shown, on top, in the from of Eq. (5) and, at the bottom, in the form of Eq. 8. (a) The single attractor at $\omega = 0$ for negative α bifurcates in a pitchfork bifurcation into (b) two symmetric attractors for turning left or right at positive α. This bistability generates hysteresis, which ensures that a decision to turn either way persists sufficiently to suppress oscillations. The symmetry of this dynamics is reduced by adding a constant term proportional to the obstacle forces, F_{obs}. In (c) this constant is positive, enlarging the basin of attraction of the attractor at positive turning rate, but maintaining bistability. In (d) the obstacle forces are so large and positive that the attractor at negative turning rate has undergone a tangent bifurcation and the system is now exclusively governed by the attractor at positive turning rate.

surrounding reflective surfaces). In the next section we show, nevertheless, how a dynamics for the turning rate, $\omega = \dot{\phi}$, can be defined that has the adequate attractor to achieve target acquisition. Thus, integrating obstacle avoidance and target acquisition involves integration of dynamics at two different orders of temporal derivative of the dynamical system. To achieve this, we must find a way to lift the dynamics for obstacle avoidance from the level of ϕ to the level of $\dot{\phi}$.

This lifting can again be based on the basic concepts of the dynamic approach. We must ask which state at the level of ω is specified by the obstacle contributions and can then use bifurcation analysis to select the adequate functional form.

Quite simply, while the heading direction is outside the repulsion zone around each detector direction or when obstacles are very far way ($\lambda_i \approx 0$), obstacle contributions Eq. (1) are small ($f_{\text{obs}} \approx 0$) and do not specify any change of heading direction. This can be expressed by specifying an attractor for a dynamics of ω at $\omega = 0$ ("move straight ahead"). Inside the repulsion zone at sufficient strength of the contribution, the attractor at $\omega = 0$ must turn into a repellor. This transition can be modelled by a pitchfork bifurcation, which stabilizes two new attractors at positive and negative turning rates $\pm\omega \neq 0$. Its normal form

$$\dot{\omega} = \alpha\omega - \gamma\omega^3 \tag{5}$$

is illustrated in the top row of Fig. 3. (see, e.g., [7], for the mathematical background). At $\gamma > 0$ fixed, the dynamics is switched by α from a regime with a single fixed point attractor at $\omega = 0$ ($\alpha < 0$, top left in Fig. 3) to a regime with two fixed point attractors at $\pm\sqrt{\alpha/\gamma}$ (turning either left or right) ($\alpha > 0$ top

right in Fig. 3). Thus, α must change sign as function of whether the obstacle contributions are sufficiently weak or not and as a function of whether or not the current heading direction is in the repulsion zone of the obstacle contribution. A systematic way to construct such a function is to integrate the force-let, which leads to something like a potential function

$$V = \sum_i \left(\lambda_i \sigma_i^2 \exp\left[-\frac{\theta_i^2}{2\sigma_i^2} \right] - \frac{\lambda_i \sigma_i^2}{\sqrt{e}} \right) \tag{6}$$

of the obstacle avoidance dynamics (see middle panel in Fig. 2). Positive values of this potential indicate that heading direction is in a repulsion zone of sufficient strength, λ_i, so that $\alpha > 0$ is required. Negative values of the potential indicate that heading direction is either outside a repulsion zone or repulsion is weak, so that $\alpha < 0$ is required. Applying a sigmoid threshold function to the potential such as

$$\alpha = \arctan[c \; V] \tag{7}$$

therefore generates the desired transition behavior. The parameter c determines the size of the transition zone. This function is illustrated in Fig. 2 to the right.

This analysis was entirely local to $\omega = 0$. It did not take into account that in the presence of repulsive forces these also specify something beyond the immediate vicinity of zero turning rate. In fact, from the sign of the obstacle forces, F_{obs}, we can read off, if an attractor at positive turning rate or an attractor at negative turning rate should be stabilized. Again, it is useful to think of the limit in which a bifurcation is generated: for sufficiently positive obstacle forces we want to eliminate the attractor at negative turning rates so that only an attractor at positive turning rates remains. Reversely, for sufficiently negative obstacle forces the attractor at positive turning rate must disappear. These bifurcations are tangent bifurcations, the normal form of which is $\dot{\omega} = \text{constant} - \omega^2$ where the constant is positive for positive obstacle forces and negative for negative obstacle forces. To integrate this with the pitchfork bifurcation, we only need to add the constant term (the higher-order terms covering the rest). To compute the constant, we multiply the obstacle forces, F_{obs} with $\alpha + \frac{1}{2}\pi$, which is zero wherever the obstacle contributions fall below a threshold. This way the attractor at $\omega = 0$ is not shifted unnecessarily when obstacle contributions are weak. The resultant dynamics

$$\dot{\omega} = (\alpha + \tfrac{1}{2}\pi) c_{\text{obs}} F_{\text{obs}} + \alpha\omega - \gamma\omega^3 \tag{8}$$

is illustrated in the bottom row of Fig. 3 for two different positive values of F_{obs}. On the left, the positive obstacle forces enlarge the basin of attraction of the attractor at positive turning rate. The attractor at negative turning rate continues to exist, however, so that the system is stabilized by hysteresis if it arrives at this situation while turning right. For even larger positive obstacle forces, the attractor at negative turning rate is eliminated by a tangent bifurcation (the dynamics lifts off the ω-axis) and the attractor at positive turning rate is monostable.

Fig. 4 summarizes the situation by showing the four regimes arising from a single, finite strength force-let: (1) Outside the range of the force-let a monostable dynamics with an attractor at $\omega = 0$ ("move straight ahead"). (2) To the right of the direction, ψ_i, into which the detector looks, negative values of f_{obs} specify turning right, corresponding to an attractor at a negative value of $\omega < 0$[2]. (3) To the left of that direction, positive values of f_{obs} specify turning left, corresponding to an attractor at a positive value of $\omega > 0$. (4) In the center zone, that is, for heading directions close to ψ_i, turning either left or right is specified, expressed as a bistable dynamics of turning rate with attractors at finite $\pm\omega \neq 0$. The transition from the center zone into either of the neighboring zones is a tangent bifurcation, while the transition to the outer zone is continuous and does not involve an instability. The pitchfork bifurcation emerges as the strength, λ_i, decreases with increasing sensed distance.

The design is completed by a formal analysis of the phase diagram of the complete second order dynamics. Heading direction, ϕ, itself is always marginally stable. Turning rate, ω, is stable at either zero or one of the non-zero values. The parameters are constrained by the requirement that relaxation be sufficiently fast so that the system is at all times in its attractor. At first sight, this might appear to be a vacuous condition, since the time units of the behavioral dynamics are really arbitrary. This requirement, nevertheless, constrains the

[2] Note that we use the mathematical convention for direction so that heading direction increases for counterclockwise rotation (turning left).

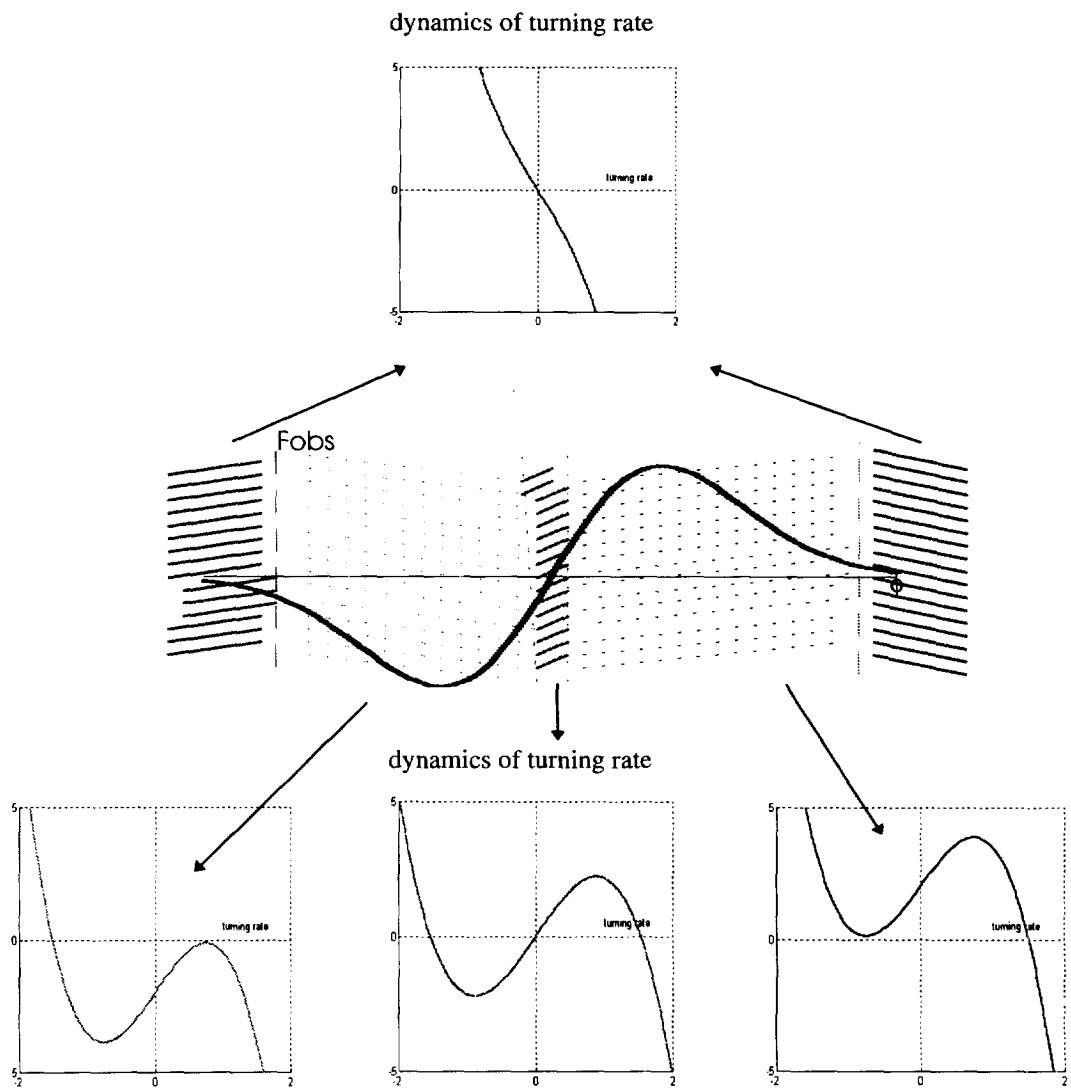

Fig. 4. This figure illustrates how the different regimes of a single repulsive obstacle "force-let" (depicted at the center) are modelled at the level of turning rate. The outer regime far from the specified direction leads to a monostable dynamics of turning with an attractor at zero turning rate (top). For the direction in which the sensor points (center region) a bistable dynamics with attractors at a positive and a negative turning rate, and a repeller at zero turning rate is erected (bottom center). In the regime of negative obstacle force (left) a dynamics with an attractor at negative turning rates is defined (bottom left). Correspondingly, for positive obstacle force an attractor at positive turning rate is defined (bottom right).

system because the time units of the dynamics are limited by the realizable sensory throughput and by the computational cycle. Specifically, time scales must be chosen such that given the computational cycle (during which sensory information must be updated), the dynamics is numerically stable. Therefore, relaxation times must be larger than the computational cycle time. The constraint that the dynamics has relaxed then in turn limits the achievable turning rates of the vehicle (cf. also Section 5).

A separate problem arises, however, because the system is moving forward in a structured environment

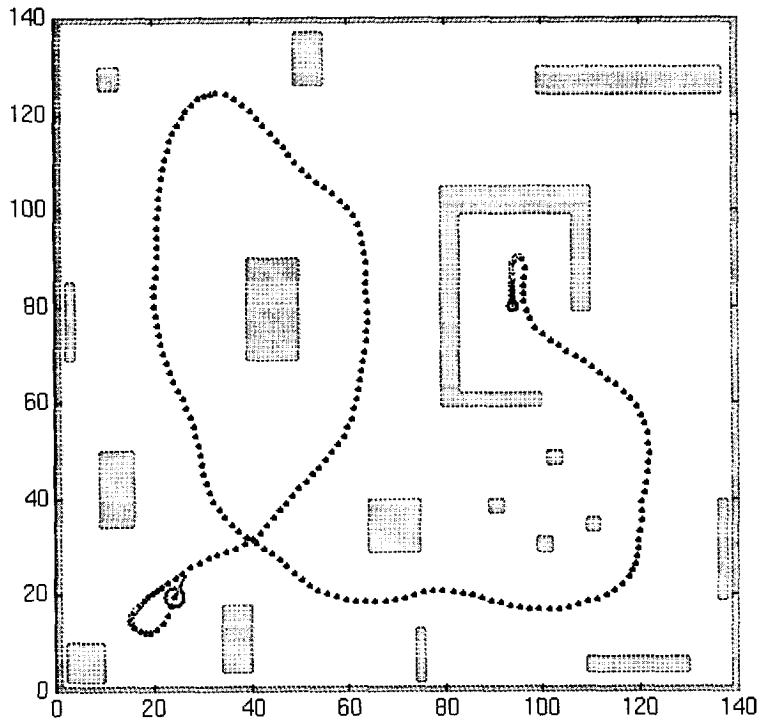

(a)

Fig. 5. Runs generated from a software simulation of the obstacle avoidance dynamics are shown. The simulator was written in MATLAB. The sensor model here consisted of measuring directly the distances from the robot to obstacle surfaces in the directions of the five vehicle mounted IR detectors. The vehicle is illustrated in its final position by a circle with a hair indicating its heading direction. The path is shown as a sequence of points. The initial robot position is indicated by a small circle. The outer perimeter and the shaded regions are simulated obstacles. Part (a) shows a run based on the first-order dynamics Eq. (4), part (b) shows a run based on the dynamics lifted to second order Eq. (8).

so that sensory information is time-dependent. Relaxation to the attractor can be enforced only if we have some handle on the rate at which sensory information might change. That rate of change can be specified by controlling the forward velocity, v, of the vehicle such as to stabilize a particular "time-to-contact", $T_{2c} = d/v$, where d is the distance to any obstructions sensed in the current heading direction of the vehicle. For the obstacle avoidance behavior, velocity control consists of simply setting driving speed to $v = d/T_{2c}$, although a more complete dynamic analysis will be required to integrate multiple constraints on velocity (see below).

In Fig. 5(b) we illustrate that this second-order obstacle avoidance dynamics works in simulation equally smoothly and in similar fashion as the first-order dynamics first implemented.

3. Target acquisition dynamics: photo-taxis

As a simplest form of sensory driven target acquisition we implement the task of photo-taxis, that is, the task of moving toward light sources (cf. [8] for the biological background). This obviates the need for explicit representation of ego-position and its updating through dead-reckoning or other means (but see [12] for a dynamic approach toward such ego-position representation). The idea is, essentially, to provide a dynamic version of Braitenberg's proposal [1]. Braitenberg pointed out that the mere feedforward connection of two light sensors, mounted side by side, to two motors, driving the wheels of a single axle vehicle, can be organized to generate phototaxis. For instance, the left light sensor might be connected to the left wheel such as to drive the wheel the faster the less

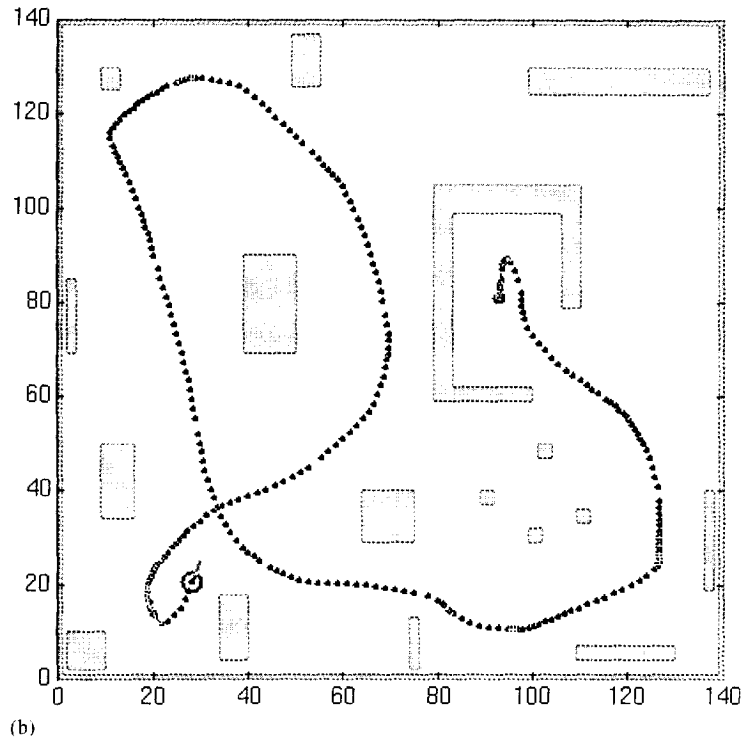

Fig. 5. Continued

light is sensed, and, correspondingly, the right light sensor would drive the right wheel the faster the less light is sensed. This leads to that wheel turning faster, on the side of which less light is sensed, so that the vehicle turns toward the brighter side. The result is orientation toward light sources, that is, photo-taxis.

This proposal can be implemented quite directly using, for instance, simple feed-forward neural nets. Two problems must be addressed, however. First, such simple taxis behavior must be integrated with other behavioral constraints, here, for instance, with obstacle avoidance. Second, and relatedly, the properties of the taxis behavior must be characterizable so as to determine parameter values on a rational basis and to specify the temporal and spatial limits within which performance can be guaranteed. Both problems are solved by implementing the Braitenberg proposal within the dynamic approach. Integration with obstacle avoidance is discussed in Section 4. The resultant behavior can be characterized in terms of linear stability theory. Because these dynamics in isolation do not undergo bifurcations, the result is equivalent to standard control theoretic solutions. The present formulation lends itself to integration with the obstacle avoidance module (cf. Section 4).

Light intensity, I_i, is sensed by two photoresistors (LDRs), one mounted on the left, one on the right side of the vehicle (i = left or right). The output voltage of these LDRs is a monotonically decreasing function of light intensity. Because of the intensity of the light source, the geometry of surfaces in the surround and their reflectances are all unknown, the LDRs cannot be said to specify a direction in space in which the target lies. Translating Braitenberg's proposal into dynamics, we can say, however, that each light specifies a turning rate. For instance, the left LDR could be construed to specify turning to the right, the rate increasing with voltage (that is, decreasing with light intensity): $\omega_{\text{left}} = -c_{\text{target}} I_{\text{left}}$ (keep in mind that ϕ is mathematically positive, so that negative $\omega = \dot{\phi}$ means turning right). The right LDR, correspondingly, specifies turning to the left at a rate that increases with voltage, $\omega_{\text{right}} = c_{\text{target}} I_{\text{right}}$. Thus, when the left sensor receives more light than the right sensor, I_{left} is

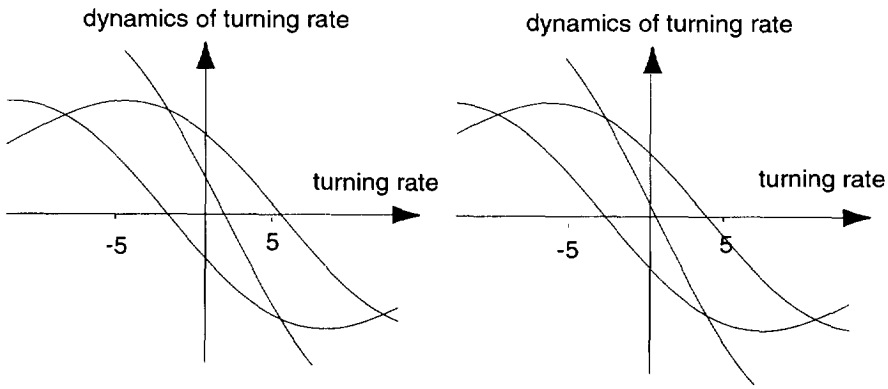

Fig. 6. Two contributions for photo taxis to the dynamics of turning rate are superposed (steeper middle curve) leading to an attractor at an averaged turning rate because we use a rather broad range functions. On the left, the right sensor receives much less intensity than the left sensor, which leads to an attractor at positive turning rates. On the right, both sensors are similarly stimulated leading to an attractor close to zero turning rate.

smaller than I_{right} and hence the rate of turning right is smaller than the rate of turning left. The vehicle would turn left toward increasing light intensity.

The averaging among the two specified turning rates is, obviously, done by a dynamical system

$$\dot{\omega} = g_{\text{taxis}} = g_{\text{left}}(\omega) + g_{\text{right}}(\omega) \tag{9}$$

with two additive contributions, each defining an attractive force-let (i = right or left)

$$g_i(\omega) = -\frac{1}{\tau_\omega}(\omega - \omega_i)\exp\left[-2\frac{(\omega - \omega_i)^2}{\Delta\omega^2}\right]. \tag{10}$$

As illustrated in Fig. 6, we use a broad range function ($\Delta\omega$ larger than the maximal values of ω_i) to average these two forces.

The time scale of this taxis dynamics is parametrized by τ_ω. Relaxation must be faster than the rate at which sensory information changes, but slower than the relaxation process driven by obstacle contributions (see Section 5). Because τ_ω defines the overall times scale of turning rate in the absence of obtacles, and this time scale is slower than that of obstacle avoidance, this limits further the maximally realizable turning rates, and thus constrains the choice of c_{target}. Again, the limit is real only because the a priori arbitrary time scales of the dynamics are delimited by the minimal realizable cycle time of sensory information acquisition and computation.

The change of sensory information due to the actual driving itself can be controlled by stabilizing a time-to-contact, again by setting $v = d_{\text{target}}/T_{2c}$. In this case, the estimate of distance to the target, d_{target}, is completely uncalibrated, of course, because it depends on the unknown intensity of the light source and the average reflectance of the surround. This does not matter for the maintenance of a slowly varying time-to-contact, although the level at which time-to-contact is stabilized may vary by as much as the light intensities in the surroundings vary. In fact, the robot moves slowly in a bright environment and faster in the dark (much like Braitenberg's first vehicle [1]). This dependence could be eliminated in an obvious manner by adaptive parameter change and measurement of ambient light level.

For the present purposes, we computed analytically the permissible ranges of values of the parameter values based on stability analysis and the time scales relationships sketched. We chose values within those ranges arbitrarily. The functionality of taxis was verified in simulation work, which used a simple distance-light intensity map to simulate the light sensor (see Section 5), not taking into account the geometry of reflecting surfaces. The implementation on the robot worked with the same parameters as used in simulation. Taxis worked fine in both simulation and reality (cf. Section 5).

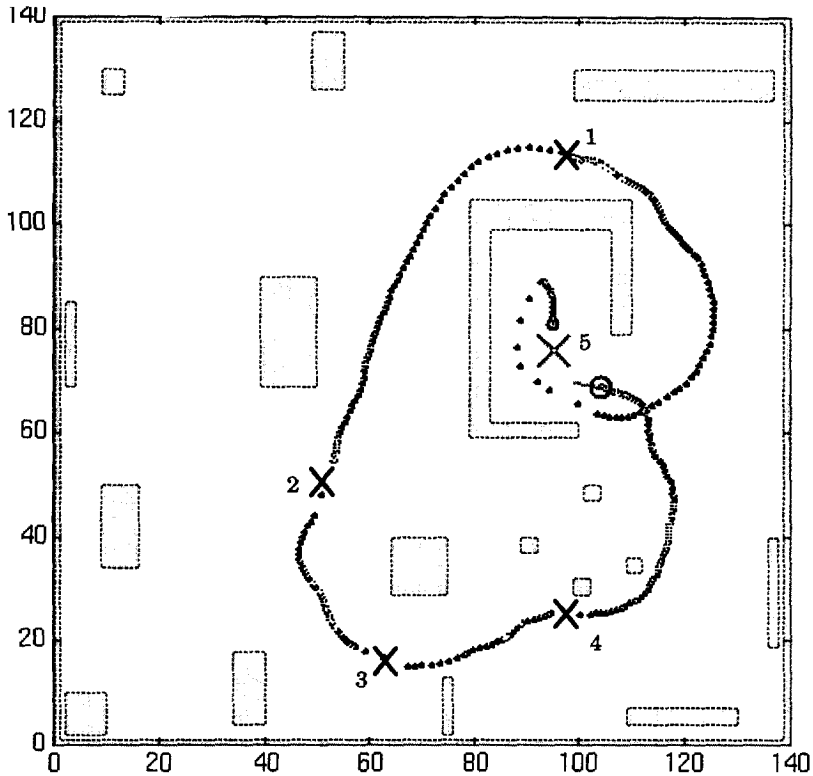

Fig. 7. This shows a run of the complete behavioral dynamics implemented in software simulation. The same conventions as in Fig. 5 apply. The light sensor is modelled by assuming that within an angular range of 75°, light intensity falls off linearly with the distance between light sensory and light source. The sensors are assumed mounted at a distance of R_{robot} symmetrically and forward-looking. Initially, the robot is inside the "box" heading toward a light source indicated by a cross marked "1" outside the box. The obstacles are assumed not to block vision. The obstacle avoidance contribution steers the vehicle out of the box toward the target. Once the target is reached, the simulated light source is shifted to the position marked by a cross labelled "2", and so on, until target number 5 is reached again inside the box. Note that in addition to escape from a box, this simulation illustrates successful navigation of cluttered environments when moving from position 4 to position 5.

4. Integrating the two behaviors

Because we have formulated both behaviors at the level of turning rate, integration of these two behaviors consists of simply adding the corresponding contributions to the vector-field

$$\dot{\omega} = g_{\text{obs}} + g_{\text{taxis}}. \tag{11}$$

Precedence of obstacle avoidance is expressed by adjusting the time scale of obstacle avoidance to be faster than the time scale of photo taxis ($\tau_\omega < 2/\pi$). For the velocity control, integrating the two constraints forces necessitate to now make explicit the dynamic nature of this control:

$$\dot{v} = f_{\text{obst}}(v) + f_{\text{target}}(v). \tag{12}$$

Here, each contribution is a force-let centered at the required velocity, v_i, with strength, μ_i and range, σ_v: (i = obst or target)

$$f_i = -\mu_i (v - v_i) \exp\left[-\frac{(v - v_i)^2}{2\sigma_v^2}\right]. \tag{13}$$

The time scales are adjusted through choice of μ such that in the presence of strong obstacle contributions ($\alpha > 0$) the obstacle term dominates while in the absence of such contributions ($\alpha < 0$) the target term dominates.

Fig. 7 shows a simulation run of the complete system which demonstrates the smooth behavior consistent with all imposed constraints.

5. Implementation and results

For implementation of the four dynamical equations a simple Euler algorithm was written in interactive C. Because the system operates close to attractors of known stability, the maximal permissible step size can be computed from the relaxation times of the attractors (time scales of the two contributions). The required time step and the cycle time needed to make one computational step delimits the time scales of the dynamics that can be realized by the system in real time. The transformations from sensor readings to the various distance dependent strengths, ranges and speeds were stored in lookup tables. A single computational step was made for each loop of sensory information acquisition. The cycle time in this form of operation is approximately 300 ms. We used the parameter settings obtained from analytical work and tested in the simulations. The system worked immediately.

The most striking feature of the system is its smooth behavior which seems to react anticipatorily to upcoming changes. This is due to how the dynamic approach permits information from various sources to affect in a graded fashion the generated behavior.

We filmed the robot motion as viewed from top in a few simple situations (which were limited by the space available within the viewing range of the camera). Fig. 8 illustrates the robot's behavior through a sequence of video images. The situation is the simplest scenario testing the obstacle avoidance behavior by setting it in conflict with the target acquisition component: Initially the robot is separated from the target (light source) by a row of obstacles. The robot moves along a curved path around the obstacles to reach the target. In Fig. 9 we illustrate a more complex scenario. Initially, the robot is positioned in a box heading toward the right (white arrow), so that it is pointing away from the only exit from the box (at the lower left corner of the box). The light source is off during that period. The robot finds the exit and, in this case, roams around in the absence of a luminosity gradient. At some point, the light inside the box is turned on. The robot finds its way back into the box, while successfully avoiding the side walls. It ends up stopping in front of the light source. Stopping comes about due to the velocity control dynamics.

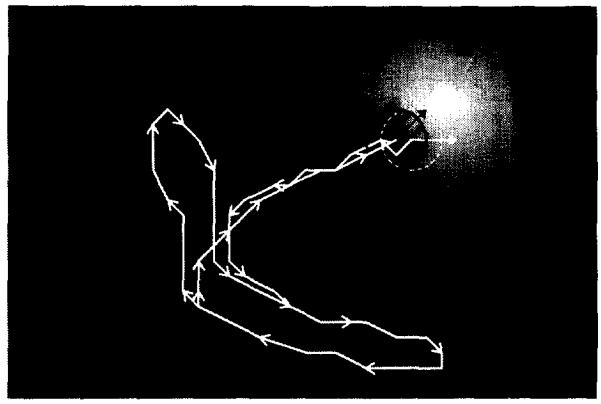

Fig. 9. This video images illustrates a more complex scenario. The initial position of the robot is shown by a dashed white circle, with a white arrow indicating its initial heading. The dark fuzzy shades are cardboard walls, enclosing the robot except for an opening near the center of the image. Initially, the light source visible in the upper right corner is off. The trajectory of the robot was reconstructed using a PC based video tracking system. The white solid line tracks out the robot trajectory, with arrows indicating the direction in which the trajectory is run through. After leaving the enclosure, the robot wanders around until the light source within the half-open box is turned on. The robot then finds its way back into the box and stops in front of the light source. The final configuration of the robot is indicated by the solid black circle and black arrow.

We also tested for oscillations near narrow passages and for escape from U-shaped obstacles. For both, performance is very good, due to the stabilization of zero-turning in the second-order dynamics. The absence of memory is a limitation, leading to meandering paths in complex obstacle arrays.

6. Conclusion

We have demonstrated that the dynamic approach can be implemented to work with very low-level sources of sensory information, here five IRs and two LDRs. This is in spite of the conceptual commitment of the dynamic approach to explicit representation of the internal behavioral state and of the behavior specified by sensory input. Moreover, a dynamic architecture including control of turning rate and driving velocity based on constraints from obstacle

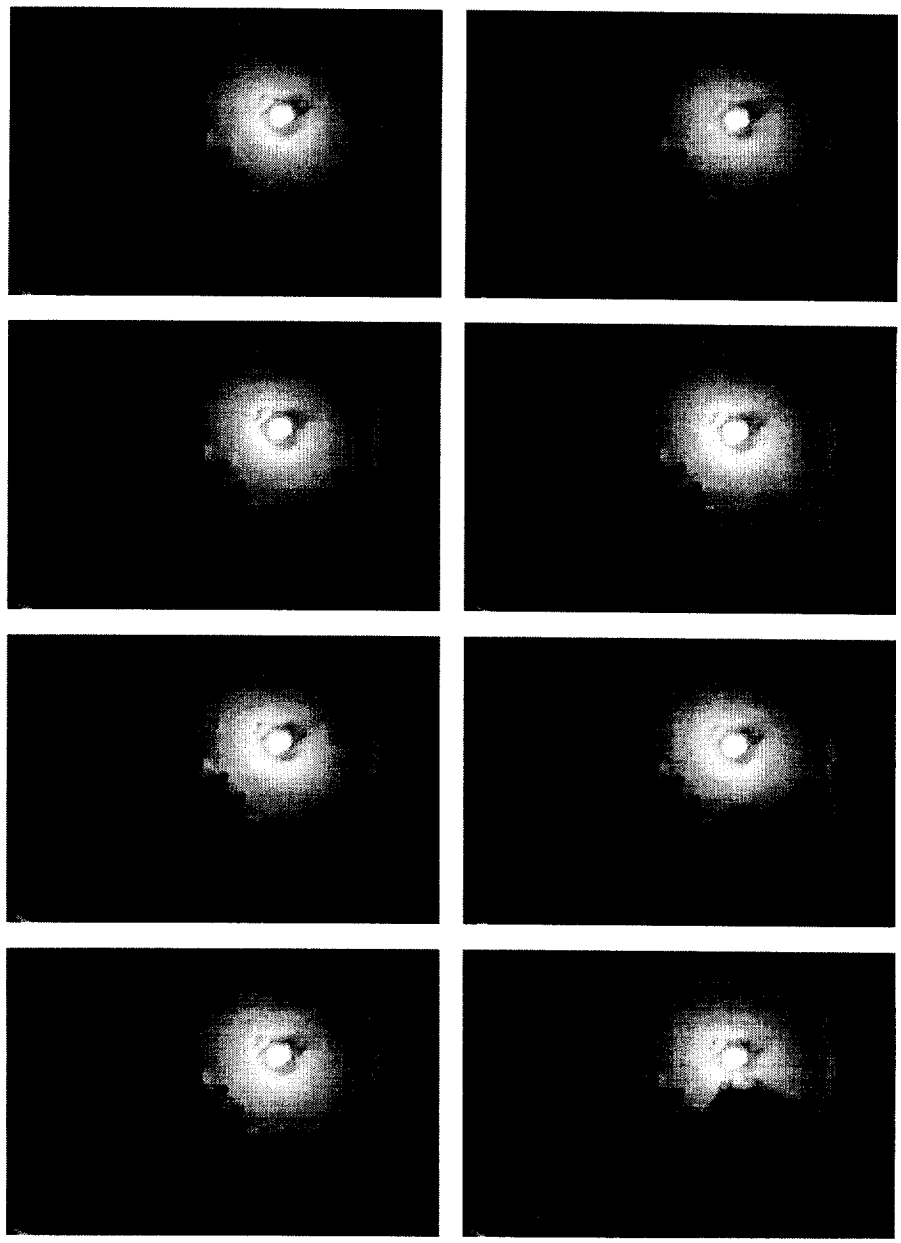

Fig. 8. A sequence of video images filmed from above illustrates the motion of the real robot. Time increases from top to bottom, first along the left column, then along the right column. The vehicle is the dark round object, located in the first frame in the lower left corner. A light source is visible in the top right corner. Four plastic cups are obstacles blocking the direct path for the robot toward the light source. The images show these cups as black dots, but the shadows are visible as well. The work space is delimited by pieces of cardboard, which are likewise detected as obstacles. The robot moves smoothly around the obstacles toward the light source, stopping in the final frame in front of the light source.

avoidance, target acquisition and the requirement to stabilizing time-to-contact was implemented on a slow 8 bit microcontroller with only 32 KByte of memory. This demonstrates that computational cost is not a limiting factor of the dynamic approach. Although we did not elaborate here for space reasons, the solution involves explicit design and specification of all system parameters based on design principles. This advantage can be exploited in future work to enable tolerance against changes in the environment by adjusting parameters adaptively.

Acknowledgements

This project was supported, in part, through grant BD/2949/94 from the PRAXIS program. We would like to thank Dr. Francisco Vaz for his support of this project and for making our collaboration possible in the first page. We thank Dr. Keith Doty and Scott Jantz for their guidance to the construction of the platform, and Dr. Couto for his institutional support. Axel Steinhage's help with the simulator and with many other matters is gratefully acknowledged as is Pierre Mallet's critical reading of the manuscript.

References

[1] V. Braitenberg, *Vehicles, Experiments in Synthetic Psychology* (MIT Press, Cambridge, MA, 1984).
[2] R.A. Brooks, New approches to robotics. *Science* 253 (1991) 1227–1232.
[3] R. Chatila, Control architectures for autonomous mobile robots, in: P. Gaussier and J-D Nicoud, eds., *Proc. From Perception to Action Conf.* Lausanne, Switzerland, 1994 (IEEE Computer Society Press, Los Alamitos, CA, 1994) 254–265.
[4] C. Engels and G. Schöner, Dynamic fields endow behavior-based robots with representations, *Robotics and Autonomous Systems* 14 (1995) 55–77.
[5] J. Jones and A.M. Flynn, *Mobile Robots – Inspiration to implementation* (A.K. Peters, 289 Linden Str., Wellesley, MA 02181, USA, 1993).
[6] H. Neven and G. Schöner, Neural dynamics parametrically controlled by image correlations organize robot navigation, *Biological Cybernetics*, in press.
[7] L. Perko, *Differential Equations and Dynamical Systems*, (Springer, Berlin, 1991).
[8] H. Schöne, *Spatial Orientation – The Spatial Control of Behavior in Animals and Man* (Princeton University Press, Princeton, NJ, 1984).
[9] G. Schöner and M. Dose, A dynamical systems approach to task-level system integration used to plan and control autonomous vehicle motion, *Robotics and Autonomous Systems* 10 (1992) 253–267.
[10] G. Schöner, M. Dose and C. Engels, Dynamics of behavior: Theory and applications for autonomous robot architectures, *Robotics and Autonomous Systems* 16 (1995) 213–245.
[11] G. Schöner and C. Engels, Dynamic field architecture for autonomous systems, in: P. Gaussier and J.-D. Nicoud, eds., *Proc. From Perception to Action Conf.* Lausanne, Switzerland, 1994 (IEEE Computer Society Press, Los Alamitos, CA, 1994) 242–253.
[12] A. Steinhage and G. Schöner, Self-calibration based on invariant view recognition: Dynamic approach to navigation, *Robotics and Autonomous Systems*, in press.

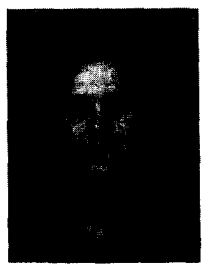

Estela Bicho (born in 1969 in Lisbon, Portugal) studied electronics and telecommunications at the University of Aveiro, Portugal, where she received her M.sc. degree in electronics in 1994 with a thesis based on a dynamic neural model for categorical perception of speech. Since then she is a research and teaching assistant at the Department of Industrial Electronics at the University of Minho, Portugal, and a member of the "Dynamics" group at the "Centre de Recherche en Neurosciences Cognitives", CNRS, Marseille, France, where she persues her doctoral studies on autonomous robotics. Research interests focus on nonlinear dynamical methods for the design, test, implementation and mantainance of autonomous robots.

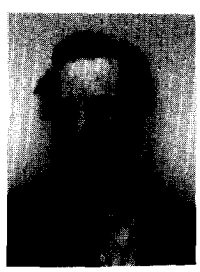

Gregor Schöner (1958) obtained a Ph.D. degree in theoretical physics from the University of Stuttgart in Germany in 1985. For the next four years he applied his background in stochastic dynamical systems to do theory on the coordination of biological movement at the Center for Complex Systems in Boca Raton, Florida. From 1989 to 1994 he led a group at the "Institut für Neuroinformatik" in Bochum, Germany, in which ideas from dynamical system theory were developed for such diverse fields as perception, movement, cortical neurophysiology, and autonomous robotics. He is now at the "Centre de Recherche en Neurosciences Cognitives" in Marseille, France, where he persues an interdisciplinary research agenda in these same fields centered around the theoretical concept of neural field dynamics.